Journal of Alloys and Compounds 501 (2010) 148–153

Contents lists available at ScienceDirect

Journal of Alloys and Compounds

journal homepage: www.elsevier.com/locate/jallcom

Nanoscale precipitates in magnetostrictive $Fe_{1-x}Ga_x$ alloys for $0.1 < x < 0.23$

Somnath Bhattacharyya[a,*], J.R. Jinschek[b], J.F. Li[c], D. Viehland[c]

[a] Dept. of Condensed Matter Physics and Materials Science, Tata Institue of Fundamental Research, 1 Dr. Homi Bhabha Road, Mumbai 400005, India
[b] FEI Company, Europe Nanoport, 5651 GG Eindhoven, The Netherlands
[c] Dept. of Materials Science and Engineering, Virginia Tech., Blacksburg, VA 24061, United States

ARTICLE INFO

Article history:
Received 10 February 2010
Received in revised form 4 April 2010
Accepted 7 April 2010
Available online 18 April 2010

Keywords:
Galfenol alloys
Magnetostrictive alloys
High resolution transmission microscopy
Line defects

ABSTRACT

We report high resolution transmission electron microscopy (HRTEM) investigations of magnetostrictive $Fe_{1-x}Ga_x$ alloys. Our findings show the presence of nanometer-sized (<2 nm) inclusions of a DO_3-like structure within an A2 matrix phase for a composition of $0.1 < x < 0.23$, whose interphase interfaces are oriented along [1 1 0]. The density of the nano-precipitates increased with increasing Ga content, however the size of the nano-precipitates was nearly independent of x.

1. Introduction

Galfenol alloys $Fe_{1-x}Ga_x$, are of considerable interests [1,2] due to very large magnetostriction coefficients along [1 0 0] (i.e., $3\lambda_{100}/2$). Both equilibrium and metastable phase diagrams are known for $Fe_{1-x}Ga_x$ [3,4]. In the equilibrium phase diagram [3], a chemically disordered body-centered-cubic bcc A2 (Fe) and ordered face-centered-cubic fcc $L1_2$ (Fe_3Ga) two phase field are present; whereas, in the metastable phase diagram [4], a two phase field between A2 and ordered bcc DO_3 (Fe_3Ga) exists. In the metastable A2–DO_3 two phase field, the value of $3\lambda_{100}/2$ depends on thermal history: with values of up to $3\lambda_{100}/2 = 400$ ppm for $x = 0.19$ at low saturation fields [5–7] when quenched. This maximum value of $3\lambda_{100}/2$ is over ten times higher than that of pure α-Fe, even though Ga is non-magnetic. A unique combination of such a high magnetostriction and a high magnetic permeability offers potential applications as sensors, actuators, ultrasonic transducers and sonar [8].

Recent theoretical studies of Fe–Ga and similar magnetic alloys have explained the unusual history dependence of the phase stability and magnetostriction based on a structurally heterogeneous state [9]. This model assumes that the heat treatment produces a structurally and chemically heterogeneous state consisting of coarsening-resistant, nanometer-scale DO_3-like precipitates within an A2 matrix. Theoretically, heterogeneity was predicted to result from the following sequence of transformations [9]: (i) bcc → bcc′ + DO_3 decomposition, followed by (ii) a diffusionless Bain strain that transforms the DO_3 nano-precipitates into a face-centered tetragonal (fct) structure which is similar to $L1_2$. Recent high resolution transmission electron microscopy (HRTEM) investigations have confirmed the presence of such a nano-dispersion of DO_3 phase nanostructures in magnetostrictive $Fe_{0.81}Ga_{0.19}$ [10]. Previously, Ikeda et al. [4] reported small DO_3 regions within an A2 matrix for Fe–19%Ga and Fe–20%Ga, which were about 40–80 nm in size. Furthermore, diffuse neutron investigations have recently indicated that the crystal structure of DO_3 nano-precipitates within the A2 matrix may in fact be distorted from cubic symmetry [11].

According to the structurally heterogeneous model [9], the two phase field of the metastable diagram of Fe–Ga should be similar to that of the chemically similar $Fe_{1-x}Al_x$ alloys [12–17]. Nano-precipitates of size 2–7 nm have been reported by electron microscopy in Fe–Al [13], where excess vacancies play a crucial role in nano-precipitate formation [9]. In this case, decomposition should only precede in the two phase field of the equilibrium (i.e., incoherent) diagram if the coherency between the phases responsible for misfit generated stresses is lifted [9]. Alternatively, if the two phases remain coherent, a metastable (i.e., coherent) phase field sandwiched between the nearest solubility lines of coherent and equilibrium diagrams has been designated as K field [16,17], as illustrated in Fig. 1a [12]. The K field is in fact a single phase field in a coherent phase diagram where coherent decomposition is impossible [18,19]: this in turn results in coarsening-resistant DO_3 nano-precipitates.

In this paper, we have examined $Fe_{1-x}Ga_x$ alloys for $x = 0.10, 0.19$ and 0.23 on the nanometer-scale using conventional TEM, as well as HRTEM lattice imaging. Our results demonstrate the presence

* Corresponding author. Tel.: +91 2222782435; fax: +91 2222804610/11.
E-mail address: somnath_tem@yahoo.com (S. Bhattacharyya).

0925-8388/$ – see front matter © 2010 Elsevier B.V. All rights reserved.
doi:10.1016/j.jallcom.2010.04.063

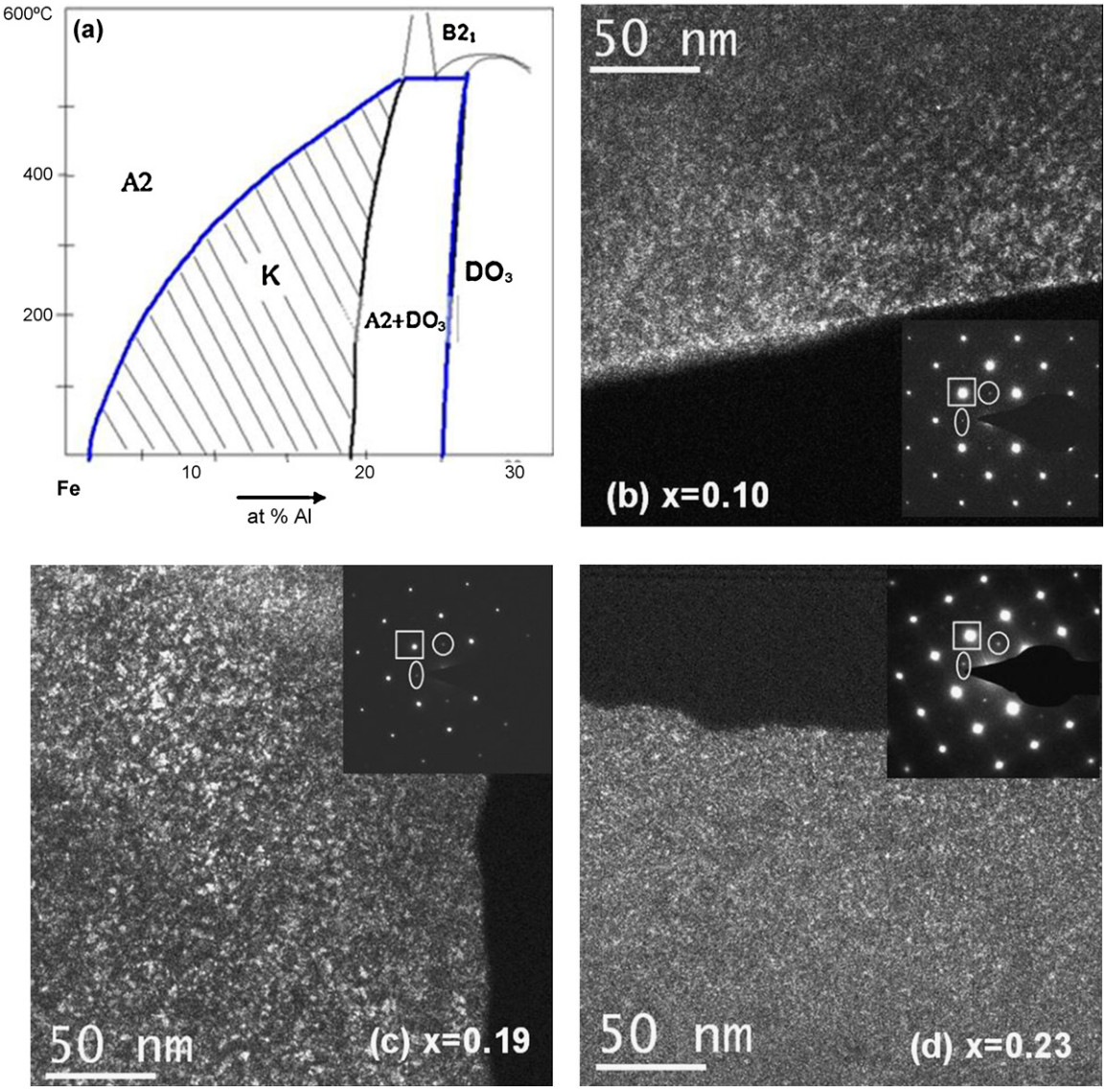

Fig. 1. (a) Phase diagram for the K field in the $Fe_{1-x}Al_x$ system [12] which is compositionally and structurally similar to $Fe_{1-x}Ga_x$ and dark field TEM images using 0 1 0 superlattice reflection of DO_3 for (b) $Fe_{0.90}Ga_{0.10}$, (c) $Fe_{0.81}Ga_{0.19}$ and (d) $Fe_{0.77}Ga_{0.23}$ alloys. Inset of (b)–(d) contain the corresponding diffraction patterns along [0 0 1] where circle, ellipse and square indicate the diffraction spots corresponding to (0 1 0), ($\bar{1}$ 0 0) and ($\bar{1}$ $\bar{1}$ 0) crystal planes respectively.

of a DO_3-like nano-dispersion within the A2 matrix over a wide range of compositions corresponding to the K field of the analogous $Fe_{1-x}Al_x$ system: where the volume fraction of the nano-dispersion for $Fe_{1-x}Ga_x$ increases with increasing Ga content x, but yet the size remains nearly constant at a few nanometers (<2 nm). Lattice imaging also revealed that the interphase interfaces between the DO_3-like nano-precipitates and the A2 matrix were all oriented along the [1 1 0].

2. Experimental procedure

Single crystal specimens were cut in a direction perpendicular to the preferred electron beam direction [0 0 1] for transmission electron microscopy (TEM) observations. Specimens were prepared utilizing the standard techniques of grinding, dimpling and argon ion-beam thinning (Model 1010 ion mill, E.A. Fischione Instrument Inc., PA, USA). Ion-beam thinning was carried out on both sides of the samples at an inclination angle of 8° of the ion-beam with respect to the sample.

The HRTEM experiments were performed using a FEI Titan™ TEM, operated at 200 kV. This microscope was equipped with a Schottky field emission gun (FEG) and a post column Gatan Image Filter (GIF) for energy filtering. Care was taken to orient the [0 0 1] zone-axis of the specimens parallel to the incident electron beam before imaging. First, we performed energy dispersive analysis by X-rays (EDAX) over numerous regions of several crystals of all three specimens. In all cases, we obtained a Ga content of stated ±0.5 at.%, clearly showing that the crystals were reasonably homogeneous.

Images were then captured onto a 1024 × 1024 pixel CCD array. The acquisition time for high resolution images was 4 s. Digital micrograph software (Gatan Inc., Pleasanton, CA, USA) was used to analyze these HRTEM lattice images.

3. Results

3.1. Dark field imaging

Fig. 1b–d shows dark field images for Fe–10%Ga, Fe–19%Ga and Fe–23%Ga specimens respectively, taken along the [0 0 1] zone-axis orientation (diffraction patterns are presented in inset) using the 0 1 0 reflection. These images were obtained from the very thin region of the samples, close to the edge of the holes produced by ion milling: this was done in order to minimize dynamic scattering effects. The 0 1 0 reflection is one of the superlattice reflection of the DO_3 structure present within the A2 matrix [10,20]. Another possible explanation for these 1 0 0 superlattice reflections could be the presence of the B2 phase: however, the B2 phase is only stable at high temperatures [3,4], and can thus be excluded.

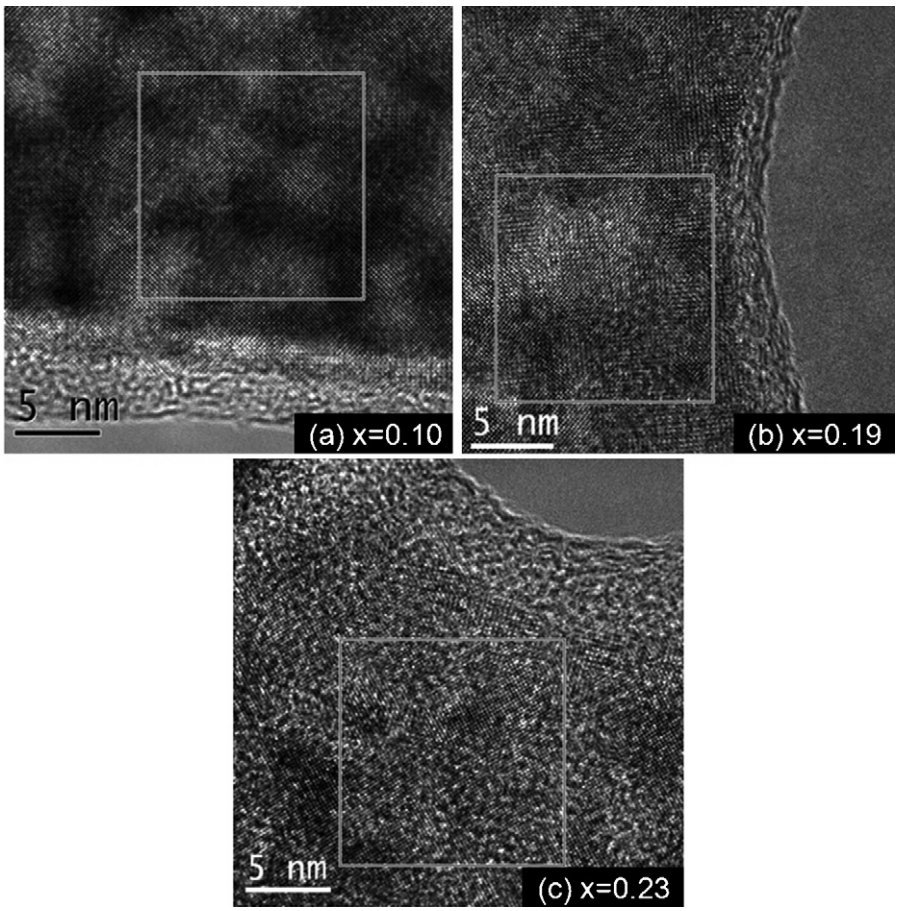

Fig. 2. High-resolution transmission electron micrograph (HRTEM) for (a) $Fe_{0.90}Ga_{0.10}$, (b) $Fe_{0.81}Ga_{0.19}$ and (c) Fe–23 at.%Ga alloys. Square boxes indicate the regions of interest, from which power spectrums were obtained in Fig. 3.

The dark field images in Fig. 1 clearly reveal a contrast consisting of a few nanometer wide bright regions within a dark matrix. This indicates the presence of DO_3 nanostructures within the A2 matrix. By analysis of the contrast, the size of these nano-regions was estimated to be in the range of 2–8 nm. By comparing these 3 images, it can qualitatively be stated that the density of the DO_3 nano-regions increases with increasing atomic % of Ga. The point-to-point resolution of the dark field images depend on the size of the objective aperture that is used in selecting the diffraction spot of interest. The radius of the objective aperture in reciprocal space used in our experiment was 0.21 $Å^{-1}$. Therefore, the resolution of the dark field images in Fig. 1 is 4.8 Å and due to this reason the DO_3 nano-precipitates sit closer than this distance can not be distinguished separately from here.

Instead of a homogeneous bcc solution, these images in Fig. 1 clearly show that the studied Fe–Ga alloys for $0.1 < x < 0.23$ consist of a nano-dispersion of small clusters. The density of these nano-precipitates increases with increasing x.

3.2. Lattice and Fourier images

Fig. 2a–c shows the HRTEM lattice images for Fe–10%Ga, Fe–19%Ga and Fe–23%Ga respectively. Power spectrums, i.e., the square of the magnitude of the complex Fourier transformation (=intensity distribution) taken from the regions defined by square boxes in the lattice images are shown in Fig. 3a–c respectively. These give detailed information about the nanostructures revealed in the dark field images.

The Fourier transforms, as well as the power spectrum of the HRTEM images, indicate spatial frequencies (i.e., g-vectors) of lattice fringes that are present and that interfere to form the lattice images in Fig. 2a–c. This Fourier analysis of different spatial frequencies points to characteristic features in a HRTEM lattice image such as the regular interference pattern, but in addition variations from this regular pattern caused by structural heterogeneity. In particular, the power spectrums in Fig. 3 reveal strong 1 1 0 reflections (indicated by solid circles) that correspond to fundamental lattice fringes common to both the disordered bcc and ordered DO_3 structures and weaker 0 1 0 ones (indicated by dashed circles) that are believed to be the g-values of superlattice fringes indicative of the DO_3 ordered structure. To analyze the origin of the weak 0 1 0 superlattice reflections in the Fourier transforms of the HRTEM lattice images in Fig. 2, an inverse fast Fourier transformation operation (IFFT) was applied by taking only the 0 1 0 g-vectors into account. In the Fourier transforms of the lattice images in Fig. 2, the weak 0 1 0 superlattice reflections of the DO_3 phase were selected by smoothed edge masks of size 1.2 nm^{-1}.

The inverse Fourier transformation of the masked superlattice reflections results in images that are interference patterns containing only the 0 1 0 spatial frequencies. Accordingly, these interference patterns contain only 0 1 0 g-vector contributions. Please note that weak 0 1 0 reflections could potentially also be caused by dynamical scattering in the A2 matrix. However, this possibility was excluded since the sample was sufficiently thin (the examined regions are very close to the edges) as evidenced by the presence of Thon rings [21] in Fig. 3a–c and by the fact

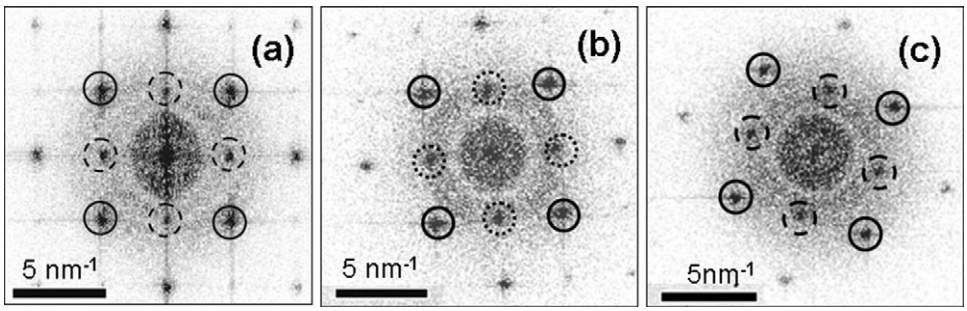

Fig. 3. Power spectrums of the regions in square boxes shown in (a) Fig. 2b for $Fe_{0.90}Ga_{0.10}$, (b) Fig. 2b for $Fe_{0.81}Ga_{0.19}$ and (c) Fig. 2c for $Fe_{0.77}Ga_{0.23}$. Solid circles show 1 1 0 reflections, dotted circles show 0 1 0 reflections.

that DO_3 was present throughout the matrix. We can thus conclude that the inverse Fourier transformed images, which were formed including only the 0 1 0 reflections, represent only the DO_3 structure. Please note that it is mainly the sharp features in the inverse Fourier transformed images that are of interest: this is because the blurred ones might be artifacts produced by Fourier transformations of masked regions. Regions of the inverse Fourier transformed images that exhibited {0 1 0} lattice fringes are shown in Fig. 4a–c (corresponding to Fig. 2a–c, respectively). Here it is worth to mention that good agreement between simulated crystal structure of DO_3 (using multi-slice) and experimental images presented in our previous work for Fe–19%Ga alloy [10] provides additional confirmation of nano-precipitates having ordered DO_3 structure.

It is important to point out from Fig. 4a–c that numerous edge line defects were present inside these nanostructures. According to our prior work [10], both negative and positive extra half planes that originate inside the DO_3 phase and the in-plane projection

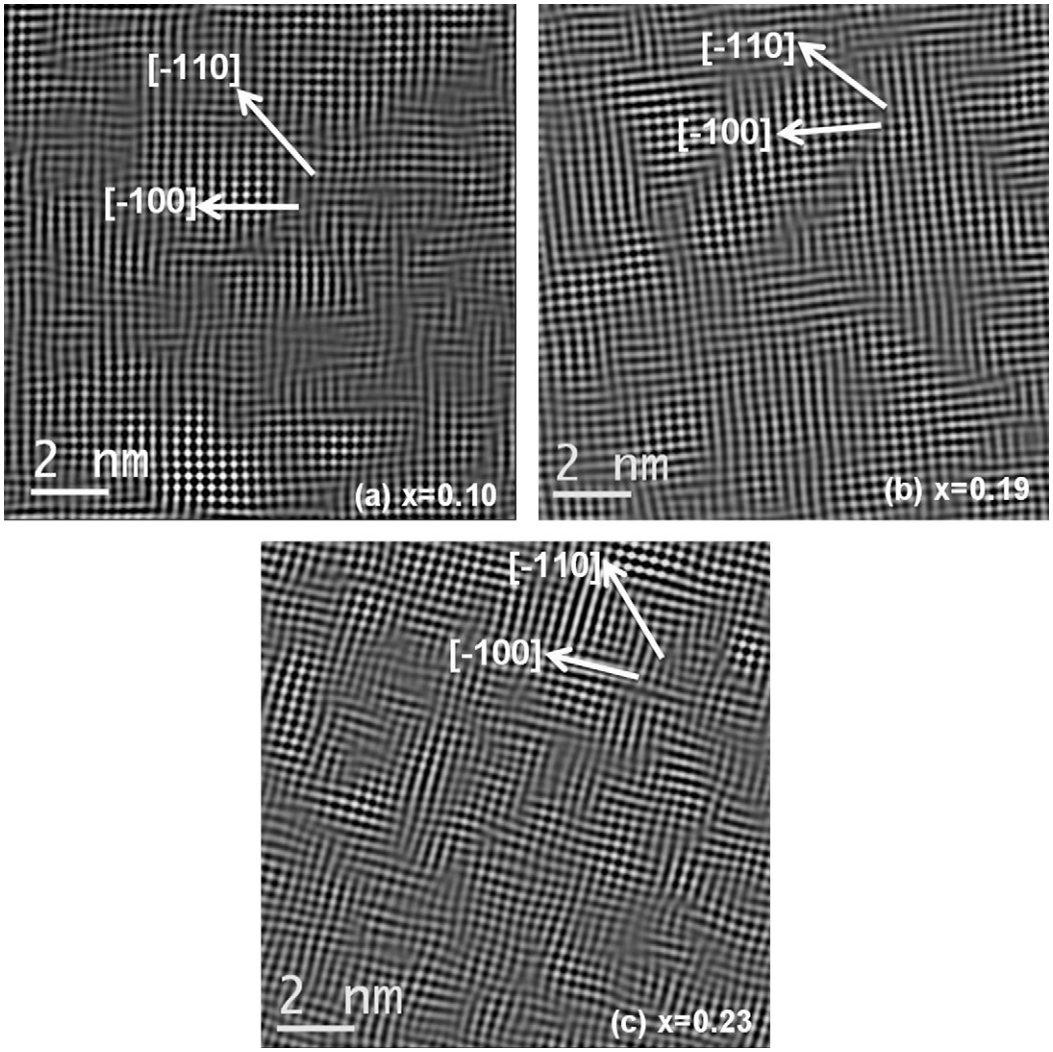

Fig. 4. Inverse Fourier transform of the 0 1 0 reflections, which were obtained from the Fourier transform of the marked region in lattice images in (a) Fig. 2a for $Fe_{0.90}Ga_{0.10}$, (b) Fig. 2b for $Fe_{0.81}Ga_{0.19}$ and (c) Fig. 2c for $Fe_{0.77}Ga_{0.23}$. These images are the interference patterns, which posses only the spatial frequencies that are contained within smoothed edge masks of size 1.2 nm^{-1} placed about the weak 0 1 0 superlattice reflections.

Table 1
Summary of analysis of inverse Fourier transformed images with regards to presence of line defects for various Fe–Ga alloys.

Alloy	Number of line defects in IFFT of 0 1 0	Number of line defects in IFFT of 0 1 0
Fe–10%Ga	17	0
Fe–19%Ga	23	0
Fe–23%Ga	56	5

of the Burgers vector of these line defects is $a/2[1\,0\,0]$. Similar [1 0 0] line defects have previously been reported for the nano-dispersion of $Fe_{1-x}Al_x$ [22]. By comparing the images in Fig. 4, we can state that the density of DO_3 nano-precipitates in Fe–Ga alloys increases with increasing Ga content, as summarized in Table 1 which reveals a qualitative comparison of number of line defects presents in IFFTs of reflections 0 1 0 (Fig. 4) and 1 1 0 (Fig. 5) taken from the similar type regions of Fe–Ga alloys with three different compositions studied in this present context. Blurred regions in all the three images of Fig. 4 directed along [1 1 0] family of directions (in Fig. 4b it is $[\bar{1}\,1\,0]$) which represent that the [1 1 0] family of directions are lacking the information of DO_3 structure. From this information it can be concluded that the interphase interfaces between the DO_3 nano-precipitates and the matrix were oriented along the [1 1 0] family of directions. This is rather unusual, as the interphase interfaces between cubic precipitates and a cubic matrix is symmetry restricted to be oriented along the [1 0 0] [19].

Next, the 1 1 0 reflections (defined by solid circles in the power spectrum of Fig. 3a–c) in the Fourier transform of the HRTEM lattice images (see Fig. 2a–c) were studied. As described above, masking tools were also applied to these spots. Inverse Fourier transformed images, formed only from the 1 1 0 spatial frequencies in masked areas, are shown in Fig. 5. Although both A2 and DO_3 structures can make contributions to the intensity of these relections (spatial frequencies), the volume of the DO_3 nanostructures inside the A2 matrix was much smaller for alloys containing 10 at.%Ga, than the other two compositions that we investigated ($x = 0.19$ and 0.23). Accordingly, it can be assumed that the image of Fig. 5a consists mostly of the A2 matrix phase. Please note, that line defects are not apparent in this image: this is in contrast to what was observed in the DO_3 phase in Fig. 3a–c. With increasing Ga content, evidence of line defects became increasingly apparent in the 110 masked IFFT lattice images. Fig. 5b for $Fe_{0.81}Ga_{0.19}$ does not directly reveal line defects, but regions where the lattice planes bend were evident; whereas, Fig. 5c for $Fe_{0.77}Ga_{0.23}$ does reveal line defects. This reflects an increased density of DO_3 nano-precipitates which also contribute to the 1 1 0 intensity.

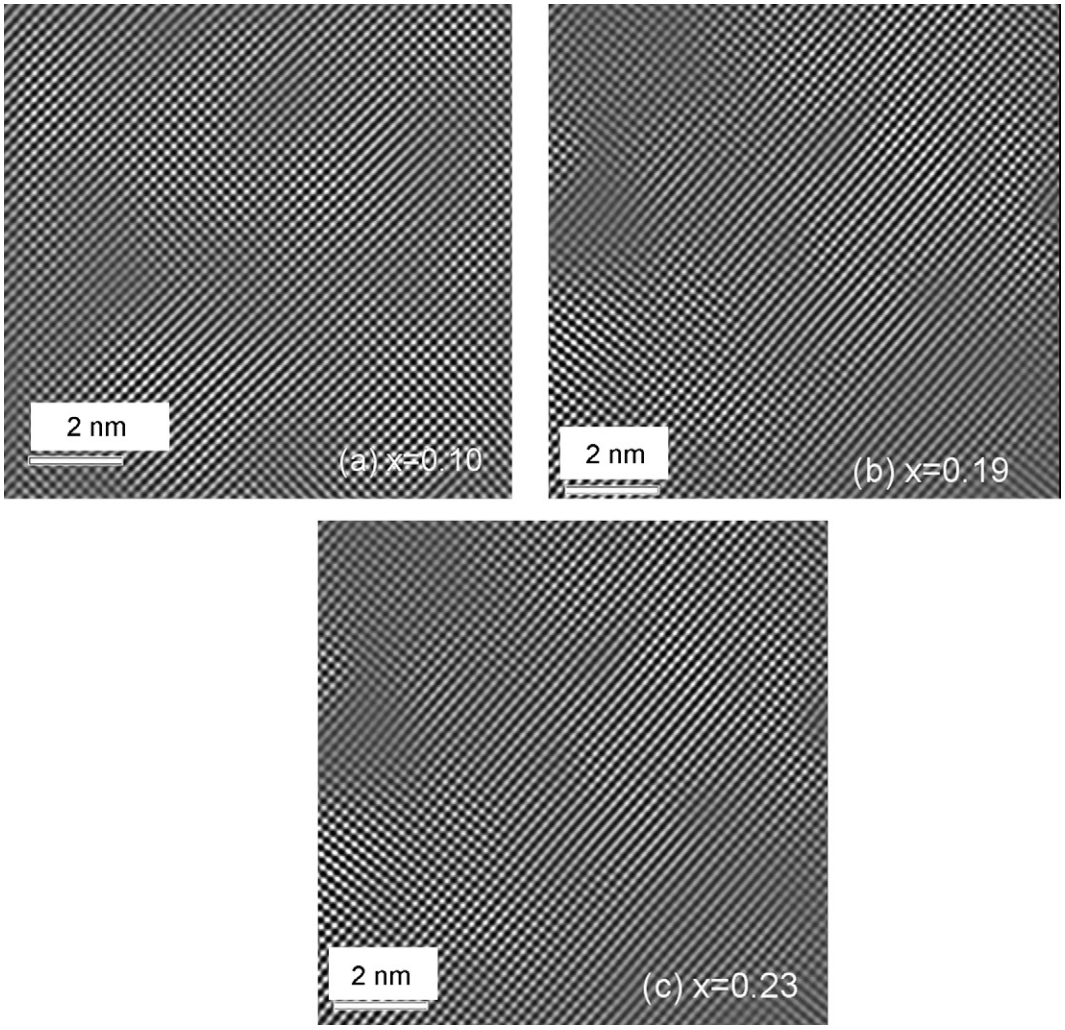

Fig. 5. Inverse Fourier transform of the 1 1 0 reflections, which were obtained from the Fourier transform of the lattice image in (a) Fig. 2a for $Fe_{0.90}Ga_{0.10}$, (b) Fig. 2b for $Fe_{0.81}Ga_{0.19}$ and (c) Fig. 2c for $Fe_{0.77}Ga_{0.23}$. These images are the interference patterns those contain only the spatial frequencies that are contained within smoothed edge masks of size 1.2 nm^{-1} placed about the strong 1 1 0 reflections.

4. Discussion and summary

Our investigations demonstrate that $Fe_{1-x}Ga_x$ alloys have a unique DO_3 nano-dispersion in an A2 matrix, similar to that previously reported for the compositionally similar $Fe_{1-x}Al_x$ alloys [12–15]. This nano-structure persists over a wide range of compositions for $0.1 \leq x \leq 0.23$, centered within what is designated in Fig. 1a as the K field. This unique state consists of a metastable equilibrium of elastically stressed phases that remain coherent with each other.

Within the compositional range of $0.1 \leq x \leq 0.23$, the volume fraction of the nano-precipitates was found to increase with increasing x. This is consistent with expectations of the application of the lever rule to the wider DO_3–A2 two phase field of the equilibrium phase diagram. These observations demonstrate that nano-precipitates persist to lower Ga contents, than originally reported [10]. It is also consistent with the previously reported enhancement in $3\lambda_{100}/2$ that occurs with continuously increasing Ga contents for $0.05 < x < 0.19$ [5–7]. The independence of the nano-precipitate size (~2 nm) with Ga content can be expected because particles of coexisting phases in the coherent system are always under a transformation-induced stress, suppressing decomposition.

We also observed that the boundaries between the DO3 nano-precipitates and the matrix were not oriented along the [1 0 0], as would be expected based on symmetry for cubic inclusions within a cubic matrix [9]. Rather, we found that these interphase interfaces were oriented along the [1 1 0], which is what would be expected of inclusions of tetragonal (or lower) symmetry that are imbedded in a cubic matrix. Recently, diffuse neutron studies have revealed asymmetric {3 0 0} peaks that have a splitting [11], consistent with the possibility that the inclusions are of lower symmetry. Furthermore, recent synchrotron X-ray investigations have shown streaking along the {1 1 0} in the diffuse scattering [23] taken around the (H 0 0) zones. It is relevant to note that these experimental patterns are similar to previous simulations of diffraction patterns in the (1 0 0) plane for a dispersion of coherent particles in a fcc cubic matrix formed by a tetragonal Bain distortion [19].

Acknowledgements

This research was sponsored by the Office of Naval Research under Grant MURI N00014-06-1-0530, and N00014-06-1-0204. The authors acknowledge support of the facilities at the Nano-scale Characterization and Fabrication Laboratory (NCFL) at ICTAS, Virginia Tech and at Department of Condensed Matter Physics and Material Science of Tata Institute of Fndamental Research, Mumbai, India.

References

[1] S. Guruswamy, N. Srisukhumbowornchai, A.E. Clark, J.B. Restorff, M. Wun-Fogle, Sci. Mater. 43 (2000) 239.
[2] A.E. Clark, J.B. Restorff, M. Wun-Fogle, T.A. Lograsso, D.L. Schlagel, IEEE Trans. Magn. 36 (2000) 3238.
[3] H. Okamoto, in: H. Okamoto (Ed.), Phase Diagrams of Binary Iron Alloys, ASM International, Materials Park, OH, 1993, p. 147.
[4] O. Ikeda, R. Kainuma, I. Ohnuma, K. Fukamichi, K. Ishida, J. Alloys Compd. 347 (2002) 198.
[5] A.E. Clark, K.B. Hathwy, M. Wun-Fogle, J.B. Restorff, T. Lograsso, V. Keppens, G. Petculescu, R. Taylor, J. Appl. Phys. 93 (2003) 8621.
[6] A.E. Clark, M. Wun-Fogle, J.B. Restorff, T. Lograsso, Mater. Trans. JIM 43 (2002) 881.
[7] T. Lograsso, A. Ross, D. Schlagel, A.E. Clark, M. Wun-Fogle, J. Alloys Compd. 350 (2003) 95.
[8] G. Engdhal (Ed.), Handbook of Giant Magntostrictive Materials, Academic, San Diego, 2000.
[9] A.G. Khachaturyan, D. Viehland, Metal. Mater. Trans. A 38A (2007) 2308.
[10] S. Bhattacharyya, J.R. Jinschek, A. Khachaturyan, H. Cao, J.F. Li, D. Viehland, Phys. Rev. B 77 (2008) 104107.
[11] H. Cao, P. Gehring, C.P. Devreugd, J.A. Rodriquez-Rivera, J.F. Li, D. Viehland, Phys. Rev. Lett. 102 (2009) 127201-1–127201-4.
[12] H. Warlimont, G. Thomas, Met. Sci. J. 4 (1970) 47.
[13] D. Watanabe, H. Morita, H. Saito, S. Ogawa, J. Phys. Soc. Jpn. 29 (1970) 722.
[14] W. Gaudig, H. Warlimont, Z. Metallkd. 60 (1969) 488.
[15] J.H. Spruel, R. Stanabury, J. Phys. Chem. Solids 26 (1965) 811.
[16] E. Ruedl, P. Delavign, S. Amelinck, Phy. Status Solid 28 (1968) 305.
[17] H. Thomas, Z. Metallkd. 41 (1950) 185.
[18] A.G. Khachatuyan, Fiz. Tverd. Tela 13 (1971) 2417.
[19] A.G. Khachaturyan, The Theory of Structural Transformations in Solids, John Wiley and Sons, New York, NY, 1983.
[20] L. Libao, F. Shiyou, L. Goudong, W. Guangheng, S. Xiudong, L. Jiangqi, Phys. B 365 (2005) 102.
[21] F. Thon, Zeitschrift fuer Naturforschung, Teil A: Astrophysik, Physik und Physikalishe Chemie 21 (4) (1996) 476–478.
[22] P. Munroe, I. Baker, J. Mater. Sci. 28 (1993) 2299.
[23] Q. Xing, Y. Du, R.J. McQueeney, T.A. Lograsso, Acta Mater. 56 (6) (2008) 4536–4546.